JACS
JOURNAL OF THE AMERICAN CHEMICAL SOCIETY
Article
pubs.acs.org/JACS

Spectroscopic Investigation of Oxygen- and Water-Induced Electron Trapping and Charge Transport Instabilities in n-type Polymer Semiconductors

Riccardo Di Pietro,[†] Daniele Fazzi,[‡] Tom B. Kehoe,[†] and Henning Sirringhaus*,[†]

[†]Cavendish Laboratory, University of Cambridge, JJ Thomson Avenue, Cambridge CB3 0HE, United Kingdom
[‡]Center for NanoScience and Technology@PoliMi, Istituto Italiano di Tecnologia, via Pascoli 70/3, 20133 Milano, Italy

Supporting Information

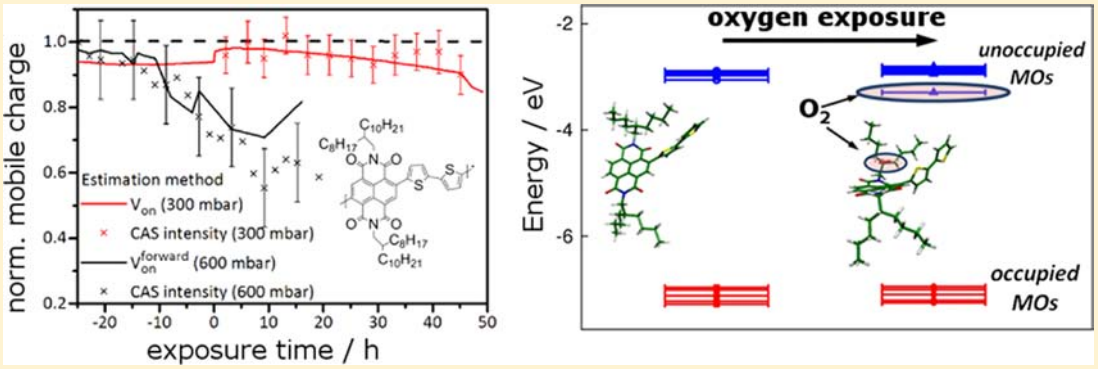

ABSTRACT: We present an optical spectroscopy study on the role of oxygen and water in electron trapping and storage/bias-stress degradation of n-type polymer field-effect transistors based on one of the most widely studied electron transporting conjugated polymers, poly{[*N*,*N*9-bis(2-octyldodecyl)-naphthalene-1,4,5,8-bis(dicarboximide)-2,6-diyl]-*alt*-5,59-(2,29-bisthiophene)} (P(NDI2OD-T2)). We combine results obtained from charge accumulation spectroscopy, which allow optical quantification of the concentration of mobile and trapped charges in the polymer film, with electrical characterization of P(NDI2OD-T2) organic field-effect transistors to study the mechanism for storage and bias-stress degradation upon exposure to dry air/oxygen and humid nitrogen/water environments, thus separating the effect of the two molecules and determining the nature of their interaction with the polymer. We find that the stability upon oxygen exposure is limited by an interaction between the neutral polymer and molecular oxygen leading to a reduction in electron mobility in the bulk of the semiconductor. We use density functional theory quantum chemical calculations to ascribe the drop in mobility to the formation of a shallow, localized, oxygen-induced trap level, 0.34 eV below the delocalized lowest unoccupied molecular orbital of P(NDI2OD-T2). In contrast, the stability of the polymer anion against water is limited by two competing reactions, one involving the electrochemical oxidation of the polymer anion by water without degradation of the polymer and the other involving a radical anion-catalyzed chemical reaction of the polymer with water, in which the electron can be recycled and lead to further degradation reactions, such that a significant portion of the film is degraded after prolonged bias stressing. Using Raman spectroscopy, we have been able to ascribe this to a chemical interaction of water with the naphthalene diimide unit of the polymer. The degradation mechanisms identified here should be considered to explain electron trapping in other rylene diimides and possibly in other classes of conjugated polymers as well.

INTRODUCTION

Since the first demonstration of n-type electron transport in organic semiconductors,[1−3] a great deal of effort has been spent to develop new materials that would allow ambient atmosphere operation of n-type organic field-effect transistors (OFETs) and other polymer-based electronic devices without suffering significant degradation of the transport properties.[4−8] These electron trapping and degradation effects manifest themselves in OFETs as a shift in threshold voltage, reduction in field-effect mobility, decrease of subthreshold slope, and increase of off-current.[9] One of the main electron trapping and degradation pathways has been found to be linked to the electrochemical reactions taking place between water and the polymer anion, with and without the presence of oxygen.[10] As an example, in the presence of both water and oxygen, the polymer anion can be oxidized according to the following reaction:

$$O_2 + 2H_2O + 4pol^- \rightleftarrows 4pol + 4OH^- \quad (1)$$

Received: May 9, 2012
Published: August 14, 2012

   dx.doi.org/10.1021/ja304198e | *J. Am. Chem. Soc.* 2012, 134, 14877−14889

This will cause the transfer of the electron from the polymer chain to an OH^- group, on which the electron will be trapped and hence not contribute to transport anymore. In a transistor device, this will lead to the formation of a matrix of fixed OH^- ions in the channel, which will contribute to the screening of the gate potential, without causing any degradation in the polymer film. Therefore, at fixed gate voltage, the amount of mobile charge available is reduced, causing a positive shift in the threshold voltage. Only a minor decrease in mobility is expected due to the additional Coulomb scattering the mobile charge would experience.[11]

The speed and direction of reaction 1 is determined by the difference between the oxidation potential of the polymer anion and the reduction potential for the half reaction involving water and oxygen. These are reported in Table 1, together with those for the corresponding half-cell reaction involving water only.

Table 1. Half-Cell Reactions with Their Standard Hydrogen Electrode (SHE) and Absolute Half-Cell Potential

half cell	$E^{standard}_{half\ cell}$/V	$E^{absolute}_{half\ cell}$/V
$2H_3O^+ + 2e^- \rightleftarrows H_2 + 2H_2O$ (SHE electrode)	0	+4.44
$O_2 + 2H_2O + 4e^- \rightleftarrows 4OH^-$	+0.40	+4.84
$2H_2O + 2e^- \rightleftarrows H_2 + 2OH^-$	−0.83	+3.61

Neglecting reorganization energies of the charged molecule and solvation/polarization effects in the solid state, the absolute oxidation potential of the polymer anion can be considered equal to the electron affinity [i.e., the energy of the lowest unoccupied molecular orbital (LUMO) level] of the neutral polymer,[12,13] and as a rule of thumb it is generally valid to assume that the higher is the electron affinity of the polymer, the higher is the stability of the polymer anion in air. According to Table 1, in the presence of water a LUMO level deeper than −3.7 eV should be sufficient to guarantee the stability of the polymer anion, while a −4.9 eV LUMO level or deeper is needed to avoid polymer anion oxidation in the presence of both water and oxygen. Possible energetic barriers for the reaction will lead to the presence of overpotentials that might enable achieving sufficient stability already for shallower LUMO levels. These considerations have channeled a lot of effort into the synthesis of new compounds with deeper LUMO energies in an attempt to make materials with improved air stability.[6−8,14−17] In addition, approaches to slow or inhibit the electrochemical reaction by increasing its overpotential have also been pursued.[18] Bulky fluorinated side chains or densely packed crystalline structures have been used to introduce kinetic barriers for the diffusion of water and oxygen molecules.[19]

As compared to the synthetic work, less effort has been devoted to the physical characterization of these instabilities. Although electrical measurements are usually performed to test whether new semiconducting materials are stable in ambient atmosphere or not,[20−22] there has been less work in trying to understand the chemical mechanism underlying degradation in these materials. In particular, while the threshold voltage shift observed in several polymers has been shown to be compatible with the degradation pathway described above,[23] at present there is no clear explanation on the causes of mobility decrease in ambient atmosphere, observed in several different naphthalene-based systems.[20,5,22] The main problems arise from the difficulty of separating the different contributions to electrical transport in field effect transistors and the lack of spectroscopic probes that are sensitive enough to directly probe the electron trapping mechanisms involved. We have recently demonstrated a new optical spectroscopy technique, charge accumulation spectroscopy (CAS), which provides spectroscopic information about degradation processes in working organic electronic devices.[24] The technique is able to determine independently the concentration of polarons in the device purely from optical measurements of their associated charge-induced absorption. This can then be compared to the results obtained from the electrical measurement and used to deduce important information on the amount of trapped charges, on their state, and on the trapping mechanism.

In ref 24 we exemplified the applications of the CAS technique by studying the degradation of poly{[*N*,*N*9-bis(2-octyldodecyl)-naphthalene-1,4,5,8-bis(dicarboximide)-2,6-diyl]-*alt*-5,59-(2,29-bisthiophene)} (P(NDI2OD-T2))[25,26] n-type OFETs in ambient/humid air. We observed a gradual loss of mobile radical anions when exposing the device to air, which was correlated with an increase of the threshold voltage, and found the observed device instability to be consistent with that expected from eq 1. However, we did not identify specific degradation pathways due to molecular interactions between the polymer and O_2/H_2O. In the present work, we focus on understanding these specific molecular pathways involved in electron trapping and degradation. For this, we have found it very helpful to investigate the separate exposure to water (without oxygen) and oxygen (without water). By preventing the fast reaction 1 from happening, we are able to study more in detail the interaction of each molecular species with the polymer.

In dry air this has allowed us to isolate a reduction in mobility and to identify its cause to be due to shallow trapping of electrons following an interaction between the neutral polymer chains and molecular oxygen. We confirmed this finding by quantum chemical DFT modeling of the interaction between molecular oxygen and the polymer chain. In a N_2/H_2O environment, the LUMO level of the polymer (−4.0 eV) should be low enough to prevent the oxidation of the polymer anion. While the oxidation of the polymer anion in this environment is indeed not a dominant effect, we observed a competing reaction involving the negatively charged polymer and water molecules, which leads to the chemical degradation of the polymer itself, irreversibly affecting charge transport in the device. In both cases, we have been able to identify the naphthalene unit as being responsible for the chemical reactions just described. The detailed molecular insight into mechanisms for electron trapping gained in this study implies important general lessons for the design of new polymers to provide air-stable electron transport.

EXPERIMENTAL SECTION

The devices used for this study are bottom-contact, top-gate transistors, made on low-alkali content, borosilicate glass. Source−drain contacts are deposited on the substrate by evaporating a 1 nm thick layer of chromium (to improve adhesion) and a 50 nm layer of gold on a photolithographically defined pattern (channel width 19.4 cm, channel length 80 μm). P(NDI2OD-T2) is spin-coated from a 9 g/L solution (90 s at 1000 rpm) and annealed for 12 h at 110 °C. The dielectric (EG-PMMA, molecular weight M_N = 300k, purchased from Polymer Source Inc.) is spin-coated afterward from a 58 g/L solution (90 s at 2000 rpm) and dried for 30 min at 80 °C. Finally, an aluminum gate electrode (10 nm thick, 0.2 Å/s evaporation rate) is evaporated through a shadow mask. A schematic diagram of the device

dx.doi.org/10.1021/ja304198e | J. Am. Chem. Soc. 2012, 134, 14877−14889

is shown in Figure 1a, together with the chemical structure of P(NDI2OD-T2).

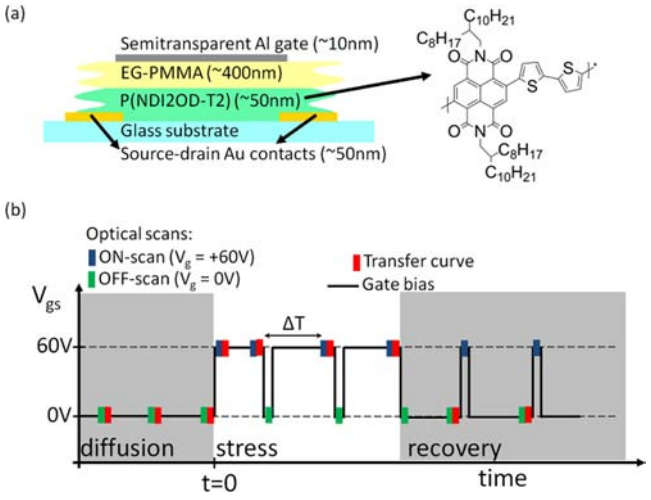

Figure 1. (a) Scheme of the transistors used and chemical structure of the semiconducting polymer P(NDI2OD-T2). (b) Diagram of the experimental measurement protocol adopted, showing the three different parts of the experiment: the diffusion of species from the atmosphere into the device with the gate grounded, the application of a gate bias (stress) to test the stability of the charged species, and the recovery upon removal of the gate bias to check the reversibility of the degradation induced by the bias stress. The black line indicates the voltage applied to the gate electrode, the blue and green dots mark when the optical spectra are taken, with a positive voltage on the gate and with the gate grounded, respectively, while the red dots show when the transfer curves are acquired.

All of the measurements are performed using a CAS system based on a commercial spectrophotometer (Agilent Cary 6000i) fitted with an Oxford Instrument CF-V continuous flow helium cryostat, modified with a needle valve to allow the purging of the cryostat with selected atmospheres. Temperature is controlled using an Oxford Instrument ITC503 temperature controller. A custom-made sample holder allows for the alignment of the active area of the transistor on the light beam path, while providing the electrical connection for the testing and stressing of the transistor. A Keithley 2612A dual channel SMU is used both for sourcing voltages and for measuring the currents flowing through the drain and gate terminals while operating the transistor in a common source configuration. Optical measurements are performed using the standard spectrophotometer configuration, in transmission geometry. The Cary 6000i spectrometer uses a continuous wave tungsten halogen light source and a InGaAs detector for the infrared (0.7−1.54 eV range) and a silicon detector for the visible (1.54−4 eV range). The spot size is approximately 0.5 × 6 mm, and the sample is aligned for the beam to fall completely inside the active area of the device (the interdigitated structure has a 4 × 8 mm area). The spectrometer has a dual-beam configuration, which allows us to continuously normalize the signal for variations in lamp intensity or other experimental conditions and achieve a high sensitivity to small changes in the optical transmission of less than 1‰. Devices are first evacuated and annealed for 6 h at 353 K to remove any trace of water from the device, thus ensuring near complete stability of the device until the vacuum is broken.[24]

The cryostat is then flushed, and the device is exposed to a controlled atmosphere. The main measurement consists of three phases (Figure 1b). In the first one (diffusion), the device is kept grounded while flushing the cryostat, to study the stability of the neutral polymer upon atmosphere exposure. In the second phase (stress), a constant gate bias of +60 V is applied, inducing an accumulation layer of electrons at the interface between the polymer and the dielectric. During this part of the experiment, the stability of the polymer anion in a particular atmosphere is analyzed. During the third phase (recovery), the device is monitored after grounding the gate. This allows one to check whether the interaction between the polymer anion and the selected atmosphere is reversible and to discriminate between interactions that involve the neutral polymer (which would continue to show the same trend during diffusion and recovery) and the reactions involving the charged polymer, which will take place only during the stress period. The origin of time ($t = 0$) is chosen as the instant when the positive gate bias is applied. The measurements acquired during the diffusion period are referred to as negative times. During the whole experiment, transfer curves (measured in continuous mode with 0.5 V steps and a 10 ms delay between steps) are acquired at regular intervals (as marked by red dots in the diagram in Figure 1b) to monitor the electrical parameters of the device. Optical scans are also acquired at regular intervals with the device grounded during the diffusion part (green dots in Figure 1b), while during the stress and the recovery segments both scans with the gate grounded and a bias applied on the gate (blue dots in Figure 1b) are obtained. No optical scan is acquired with a bias applied on the gate in the diffusion part to avoid unwanted stress effects on the device. All optical spectroscopy measurements are performed with a fixed slit bandwidth of 0.6 nm, with a resolution of 0.5 nm in the 1800−800 nm range, and a 0.1 nm resolution in the 800−300 nm range. All measurements are performed at room temperature.

CAS can be applied in two different modes. The CAS spectrum of mobile polarons in the OFET accumulation layer can be obtained by calculating the difference between two consecutive optical scans, one with the gate grounded and one with a positive bias applied. Polaronic charges in organic semiconductors exhibit characteristic charge-induced optical absorptions different from those of the neutral molecule. The intensity of these polaron-induced absorptions and of the associated bleaching of the neutral absorption can be used to quantify the amount of charge that is accumulated on the polymer film following the application of the gate bias. CAS can also be applied in a trap-sensitive mode in which it is able to detect the spectroscopic signature of residual trapped charges left in the device after removing the gate bias. This is achieved by calculating the difference between two optical scans with the device switched off, one acquired before the stress and the other one after the stress. The CAS technique is explained in more detail in ref 24.

First-principles density functional theory (DFT) calculations have been carried out to model the oxygen versus neutral polymer interaction and the corresponding changes in terms of electronic structures and charge transport levels. M06-2X hybrid functional[27] with a triple split Pople basis set with diffusion and polarization functions, for example, 6-311G(d,p), has been used. Counterpoise basis set superposition error (BSSE[28]) has been applied for evaluating the stabilization energy ΔE calculated as the difference between the total energy of the oxygen−polymer complex and the single total energies of molecular oxygen and polymer considered as separated (e.g., not interacting). The oxygen molecule has been considered in its stable triplet ground state, and a UM06-2X/6-311G** calculation has been carried out. The polymer has been studied by following an oligomeric approach, as was already reported in refs 29,30. We considered two case studies, for investigating the influence of the polymer chain length in changing the stabilization energy of the oxygen interaction and of the electronic structures: (a) the monomer (e.g., chemical unit) $(NDI2OD\text{-}T2)_1$ with alkyl chains, interacting with one molecular oxygen, $O_2\cdots(NDI2OD\text{-}T2)_1$ complex, and (b) the pentamer, for example, five repeat units with methyl groups instead of alkyl chains, interacting with one molecular oxygen, $O_2\cdots(NDI2OD\text{-}T2)_5$. The geometry of the oxygen−polymer complexes, both (a) and (b), has been fully optimized without constraints. The molecular oxygen has been set as a starting guess configuration on top of the NDI2OD core.[31] A stabilizing interaction ($\Delta E < 0$) has been found for both (a) and (b) cases, and the intermolecular NDI$\pi\cdots O_2$ equilibrium distance has been optimized around 3.0 Å. Our model strategy suggests that specific and local interactions between O_2 and P(NDI2OD-T2) π-electron delocalized structure take place, and this

dx.doi.org/10.1021/ja304198e | J. Am. Chem. Soc. 2012, 134, 14877−14889

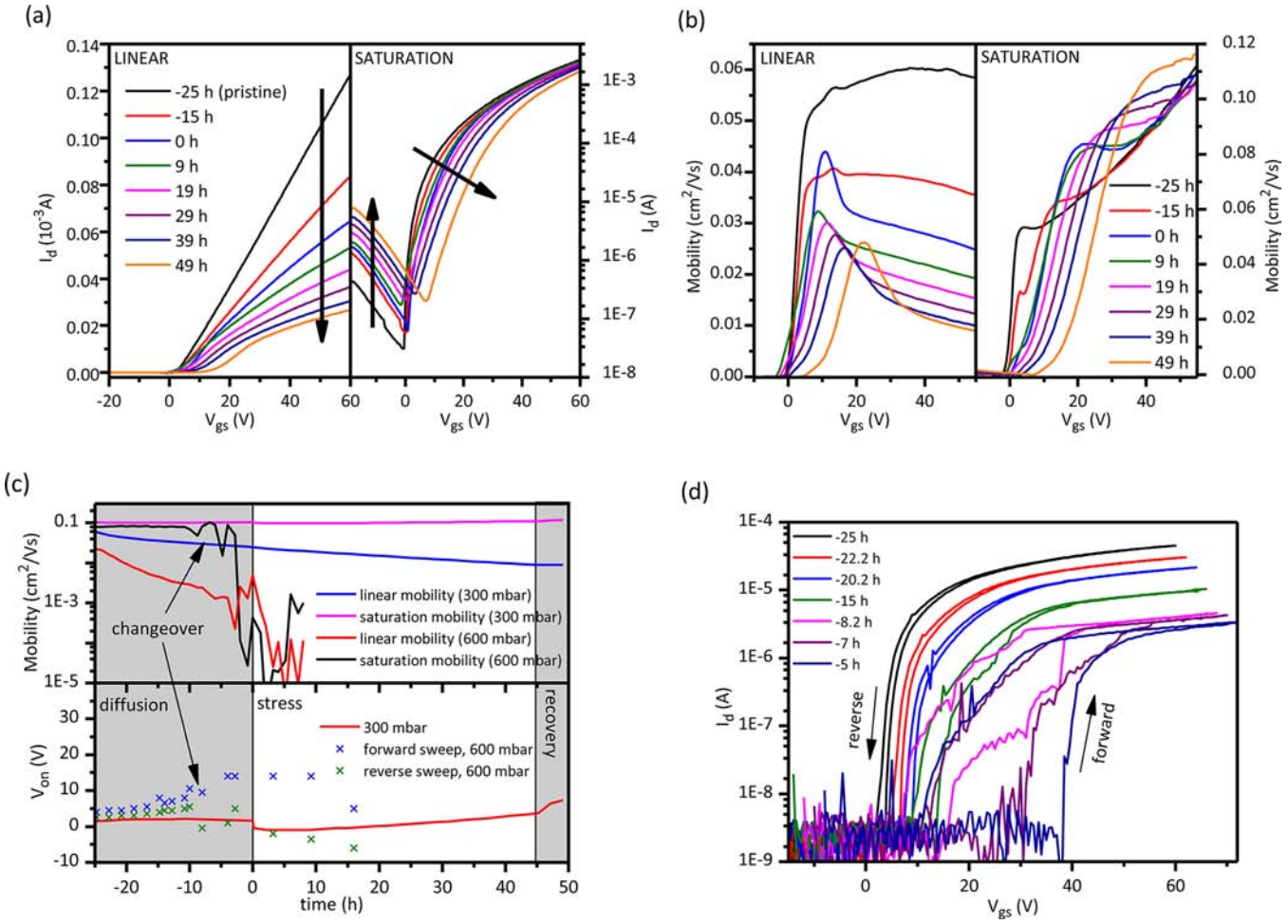

Figure 2. (a) Evolution of transistor transfer characteristics upon dry air exposure (pressure 300 mbar). Right: Linear transfer characteristic, obtained with V_{ds} = 2 V. Left: Saturation transfer characteristics, obtained with V_{ds} = 60 V. The origin of time is chosen as the beginning of the bias stress part, so that the pristine curve is obtained at t = −25 h, just before filling the cryostat with dry air. The black arrows highlight the main features and their evolution with time. (b) Gate voltage-dependent mobility curves: linear mobility is shown on the left, saturation mobility on the right. These curves are derived from the transfer curves shown in (a). (c) Evolution of the device electrical parameters with time, highlighting the different phases of the experiment. Upper graph: Time evolution of the linear and saturation mobility. Lower graph: Onset voltage time evolution. The mobility value is taken in both cases for V_{gs} = 55 V. For the 600 mbar experiment, no stress measurement has been performed. The changeover point marks a change in behavior of the degraded sample, when degradation in the device becomes too high for the transfer characteristic to be measured easily and hysteresis starts to increase. (d) Evolution of the linear transfer curves for the 600 mbar experiment, showing the increase and direction of the observed hysteresis. The traces are offset of 2 V each on the x axis for clarity.

is also supported by a recent computational investigation carried out on similar π-conjugated systems.[31]

In the Supporting Information, the excited-state calculations, carried out at the TD-M06-2X/6-311G** level for both $O_2\cdots(NDI2OD\text{-}T2)_1$ and $O_2\cdots(NDI2OD\text{-}T2)_5$ complexes, as well as for the noninteracting oligomers, are reported. TDDFT calculations, carried out to evaluate the effects of the polymer−oxygen interaction on the optical properties of P(NDI2OD-T2), support the experimental CAS results, thus predicting red- and blue-shifts for, respectively, the low and high energy absorption bands of the polymer. All calculations have been carried out by using Gaussian 09.[32]

Micro-Raman spectroscopy was performed using a WITec Alpha 300 system. The excitation laser wavelength was 532 nm, and the laser power at the sample was approximately 0.2 mW. Raman spectra were obtained in the backscattering geometry via an Olympus 50×, 0.5 numerical aperture, long working distance microscope objective. The sample was in a continuous flow of dry nitrogen gas in a Linkham stage at room temperature.

THE ROLE OF OXYGEN

To study the effect of oxygen exposure on the behavior of the semiconducting polymer, we flushed the cryostat with a certified dry air gas bottle from BOC gases (composition: O_2 20−22%, CO_2 < 2 ppm, H_2O < 1 ppm, NO_X < 0.1 ppm, THC < 0.1 ppm). We performed the first experiment with a pressure of 300 mbar inside the cryostat, and we did a control experiment on a different device with a pressure of 600 mbar, without stressing the device, because as it will be explained in the following, charge accumulation was found to have no influence on degradation with this atmosphere composition (for the same reason, we also performed both the ON and the OFF scans throughout the 600 mbar experiment, from the very beginning). The two measurements have been performed on devices from different batches, to account for sample-to-sample variations on the degradation effects.

Electrical Characterization. The pristine device, in vacuum, shows an almost ideal behavior (Figure 2a, −25 h trace), with a steep subthreshold slope and an almost straight

dx.doi.org/10.1021/ja304198e | J. Am. Chem. Soc. 2012, 134, 14877−14889

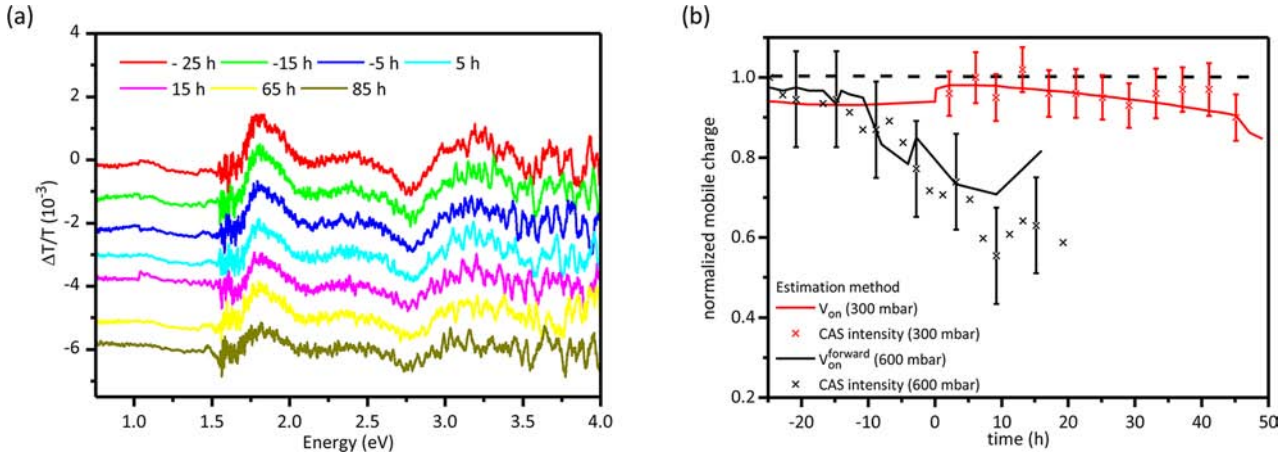

Figure 3. (a) CAS spectra of mobile polarons, obtained at different times during the 600 mbar experiment. The intensity of the signal is directly proportional to the amount of charge accumulated on the semiconducting polymer chains that react to the application of the gate voltage. For this experiment, ON and OFF scans have been acquired from the very beginning of the experiment, and also during the diffusion part. The traces are offset for clarity. (b) Evolution of the amount of charge accumulated on the polymer film, extracted both from electrical and from optical measurements.

on-region in the linear transfer characteristic, while the saturation transfer curve shows negligible hole transport (the current for negative gate voltages is comparable to the gate leakage) and a sharp turn-on at V_{gs} = 0 V.

When the chamber is filled with dry air, current starts to drop with time (−15 h trace), and a kink appears in the on-region of the linear transfer curve (0 h trace). In the saturation transfer curve, it is possible to notice a decrease of the on-current, more evident for low gate voltages (the current drop of the saturation current for 49 h trace, at V_{gs} = 60 V, is roughly 37% of the initial value measured in the −25 h trace, much less as compared to the drop in the linear transfer at the same gate voltage, which is 83% of the initial value). Interestingly, the device also becomes more ambipolar. We detect a significant increase of hole current at negative gate voltages, which becomes significantly higher than the leakage current (on the order of 10^{-7} A, with V_{gs} = −10 V and V_{ds} = 60 V) with increasing dry air exposure.

From these transfer curves, using the standard OFET equations in the gradual channel approximation, we extracted the mobility in both the linear and the saturation regime (Figure 2b).[33,34] The gate dielectric capacitance (C = 6.4 nF/cm^2) value needed to extract the mobility was obtained from a CV scan. We assumed C to remain constant throughout the measurement. The calculated mobility in vacuum is 4.8 × 10^{-2} cm^2/(V s) in the linear regime and reaches a value of 9.8 × 10^{-2} cm^2/(V s) in the saturation regime. When exposed to dry air, linear mobility decreases significantly, showing a marked peak at low gate voltages and then dropping for higher gate voltages, and the saturation mobility, while dropping for low gate voltages, as expected looking at the transfer curves in Figure 2, is roughly unaffected for high gate voltages. The evolution of these parameters with time is shown in Figure 2c, together with the values obtained for the control experiment.

The different evolution of linear mobility (decreasing) and saturation mobility (stable for the 300 mbar experiment) is the result of an increase in contact resistance in the device during dry air exposure. In particular, the formation of a peak in the gate voltage dependent mobility curve can be explained by assuming an increasing series resistance in the device with oxygen exposure, which dominates charge transport when the channel is made highly conductive at high gate voltages.[35−37] The contact resistance of staggered OFETs is determined by the interfacial potential barrier for electron injection at the metal−semiconductor interface as well as the bulk resistance of the semiconductor, which charges have to cross to reach the accumulation layer and be collected at the drain contact. The observed contact resistance behavior can be explained by assuming that oxygen exposure causes the formation of trap states, which decrease the electron bulk mobility. This also explains the shift of the peak in the gate voltage-dependent mobility to higher gate voltages because the same mechanism is also lowering the channel conductivity due to the increase in trap concentration in the channel area.

In Figure 2c, bottom graph, the onset voltage V_{on} is plotted for the two measurements. V_{on} (defined here as the voltage at which the current exceeds I_{on} = 5 × 10^{-8} A) is used instead of the threshold voltage (V_{th}) due to the transfer curves exhibiting a pronounced change in shape with exposure time (Figure 2). The small negative V_{on} shift upon bias application (t = 0 s) for the 300 mbar measurement is a completely reversible effect (see the positive shift in the recovery part) and is observed in vacuum as well. Apart from this shift, V_{on} shows only a minor increase throughout the measurement. The behavior is similar in both measurements, although as expected mobility degradation is faster for the 600 mbar experiment. In the 600 mbar experiment, we detect an abrupt change in behavior around t = −15 to −10 h (indicated with arrows in Figure 2c). At this stage, the degradation effects become sufficiently strong as to affect also the saturation mobility, and the electrical measurements begin to show an increased noise level and hysteresis (Figure 2d). We emphasize that this abrupt change in degradation behavior is caused neither by gate dielectric breakdown as the gate current remains small, nor by a degradation of the gate electrode itself, which has been checked to be still conductive at the end of the experiment. The hysteresis of the linear transfer curve (shown in Figure 2d) is reflected in different onset voltages measured in the forward and reverse gate voltage sweep direction (Figure 2c). It is initially limited to 2−3 V, but starts increasing around t = −15 h. The current is higher on the reverse sweep, which is the opposite behavior of what is normally observed in organic semiconductor.

dx.doi.org/10.1021/ja304198e | J. Am. Chem. Soc. 2012, 134, 14877−14889

Hysteresis behavior is usually associated with the formation of a high density of shallow traps in the semiconducting polymer.[38−40] We interpret the higher electron current during the reverse sweep as evidence that during the reverse sweep, electron trap levels, which were filled during the forward scan, are rapidly emptied, and this detrapping process contributes to the measured electron current. The current due to detrapping is measurable here because we use a relatively fast sweep rate in the transfer scans of 50 V/s to minimize bias stress effects being induced during the transfer scans. This hypothesis is supported by the integrated charge collected during the reverse sweep being of the same order of magnitude as the total number of "missing" electrons in the channel area as estimated from the optical measurement (reported in the following section).

Optical Characterization. In Figure 3a, we show "mobile" CA spectra obtained at different times for the 600 mbar experiment. The characteristic polaron-induced absorption (PIA) at 1.5 and 2.75 eV ($\Delta T/T < 0$), and the bleaching of the semiconducting polymer neutral absorption at 1.7 and 3.1 eV ($\Delta T/T > 0$), is the signature of the formation of a polaron state upon charge accumulation, caused by a rearrangement of the electronic energy levels following the strong polaronic interaction of the additional electron with the nuclear and electronic degrees of freedom of the molecule.[30] It can be noticed how the charge-induced absorption and the corresponding bleaching signals decrease with time, although the spectral shape is not affected. This effect is seen only for the 600 mbar experiment and not for the 300 mbar one, where the CAS intensity does not decrease significantly from its pristine value.

The intensity of the CA spectrum can be used to obtain an estimate of the charge accumulated on the polymer chains. We can compare this estimate with the mobile charge density (n_P^{mobile}) that can be extracted from the electrical measurements using the onset voltage:

$$n_P^{mobile}(t) = C(V_{gs} - V_{on}(t)) \quad (2)$$

The normalized charge density extracted with the two methods is reported in Figure 3b, for both the 300 mbar and the 600 mbar experiment. For the 300 mbar experiment, the extraction is straightforward due to the lack of any significant hysteresis in the transfer characteristics. It can be seen how, from the electrical measurements, only a minor reduction in the mobile charge density is observed. It cannot be ruled out that the small decrease in the electrical estimate may be caused by an artifact in the extraction of V_{on} caused by the pronounced decrease in mobility.

More interesting are the results for the 600 mbar experiment, for which we observe not only a contact resistance degradation, but also a shift in turn-on voltage and increasing hysteresis, suggesting significant charge trapping at the interface. To take into account the hysteresis, we estimate the residual mobile charge density from the onset voltage in the forward transfer characteristics, $V_{on}^{forward}$, using $n_P^{mobile} = C(V_{gs} - V_{on}^{forward})$. In this, we assume that the higher value of $V_{on}^{forward}$ as compared to that measured in the reverse sweep reflects the rapid filling of trap states as the device is switched on and that the electrons that are accumulated and trapped at low gate voltages do not contribute to the transistor current during the forward scan. We compared this electrical estimate with the amount of charge accumulated on the polymer film as observed with CAS, and we found that the two values are in good agreement (Figure 3b). This is consistent with all charges that remain mobile and contribute to the current in the forward scan, also contributing to the charge induced absorption signal in CAS. On the other hand, this result also suggests that the trapped electrons, which are the origin of the high value of $V_{on}^{forward}$, do not exhibit an optical charge-induced absorption similar to that of mobile radical anions on the polymer chain; that is, the electrons are not trapped on the polymer chain. If the trapped electrons were still located on the polymer chain, they should result in a charge-induced absorption, and the total CAS-induced absorption should remain constant during the experiment, because the hysteresis observed in the transfer characteristics indicates that electrons are quickly detrapped on gate bias removal. Between the CAS ON transmission scan and the OFF scan measured, immediately afterward both mobile and the shallowly trapped charges are apparently able to leave the device. At the end of the measurement sequence, up to 40% of the accumulated charge is located on a trapping site. This is additional evidence that the abrupt change in the device degradation behavior referred to above might be caused by the concentration of oxygen-induced trap sites in the semiconducting polymer becoming comparable to the accumulated charge carrier concentration.

We have also taken CAS spectra at zero gate voltage at various times during the diffusion and stress sequence and referenced these against the original transmission spectrum measured prior to any dry air exposure at $t = -25$ h (Figure 4).

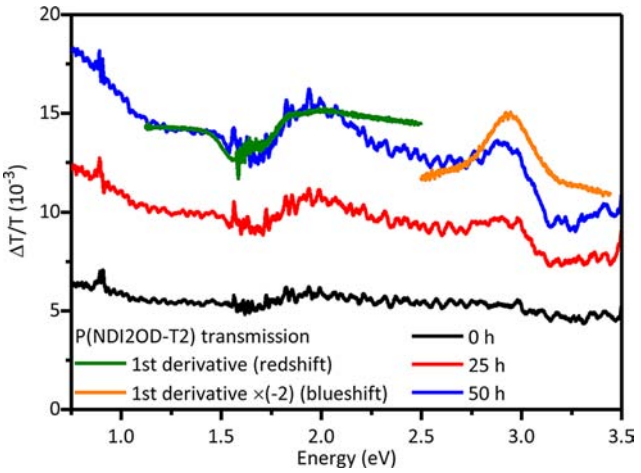

Figure 4. Evolution of the device transmission spectrum during dry air exposure at 300 mbar. The spectra were obtained with the gate grounded at $t = 0$ h, $t = 25$ h, and $t = 50$ h and referenced against the transmission spectrum of the pristine device at $t = -25$ h prior to any dry air exposure. The first derivative of the polymer film transmission spectrum is superimposed on the spectrum obtained after 50 h stress. The measurement refers to the experiment performed at 300 mbar pressure.

They should be sensitive to any induced absorptions from long-lived trapped charges or any oxygen-induced changes of the polymer absorption/transmission spectrum. All three spectra show the same features with mainly the magnitude of the signal changing. The positive and negative peaks in these spectra, although related to the polymer optical transitions, have slightly different energies with respect to the neutral polymer absorption peaks.[30] A chemical degradation of the neutral polymer, with a disruption of the π-orbital conjugation, would only lead to a bleaching of the neutral absorption peaks, which

would then show up in these spectra only as positive peaks at different energies from the ones observed (see water section, Figure 8c).

However, the observed spectral features are instead related to the first derivative of the polymer transmission spectrum (Figure 4, green and orange trace). A red-shift of the neutral absorption would decrease the transmission just below the neutral absorption and increase it just above, and will therefore have a spectrum similar to the first derivative of the absorption spectrum (green trace). A blue-shift would show the opposite feature, increased transmission below and decreased transmission above the absorption edge, with a shape similar to the inverse of the first derivative of the absorption spectrum (orange trace).[41,42] The low energy feature around 1.7 eV in the CAS spectrum in Figure 4 can be explained by a small red-shift of the neutral polymer absorption, while the high energy feature around 3 eV can be explained by a small blue-shift of the neutral polymer absorption in the presence of dry air. This result indicates that rather than inducing chemical degradation of the neutral polymer, the interaction with oxygen is causing a slight rearrangement of the oscillator strength for both the low and the high energy optical transitions of the neutral polymer.

Quantum Chemical Calculations of O_2···P(NDI2OD-T2)$_n$ Interaction. The experimental evidence obtained in dry air indicates that degradation is due to an interaction between molecular oxygen and the neutral polymer segments, taking place in the whole bulk of the semiconducting layer even in the absence of charge accumulation. As shown by CAS, this interaction does not cause any chemical degradation of the neutral polymer involving the formation of chemical defects, but results in the formation of shallow electron traps, which initially cause a reduction of the bulk electron mobility affecting contact resistance and, at higher concentrations, lead to a reduction of the mobile charge density in the channel and the onset of hysteresis in the transfer characteristics.

To investigate the microscopic nature of the trap state(s), we performed DFT (M06-2X/6-311G**) calculations to model the interactions between molecular oxygen (O_2) and the polymer chain. As described in the Experimental Section, we performed DFT calculations on two different configurations, the monomer unit of P(NDI2OD-T2) interacting with one O_2 molecule on top of the NDI moiety (O_2···(NDI2OD-T2)$_1$ configuration a) and a pentamer (NDI2OD-T2)$_5$ interacting with one O_2 on top of the central NDI unit (O2···(NDI2OD-T2)$_5$ configuration b).

Geometries have been fully optimized without constraints. Counter poise BSSE interaction energy has been evaluated for the stable optimized O_2···polymer structures to be around −5.64/−6.00 kcal/mol. The value of the interaction energy could be slightly overestimated due to approximations in the DFT functional and basis set adopted; nevertheless, the calculated values suggest moderate oxygen−polymer interactions in the film that might be reversible due to their moderate strength during thermal treatment or mere diffusion. Figure 5 reports the stable optimized structure found for O_2···(NDI2OD-T2)$_1$ complex, with molecular oxygen in a stable minimum of the potential energy surface at an intermolecular distance around 3 Å.[31]

Upon interaction, modifications in the P(NDI2OD-T2) electronic structure take place. For both cases (a) and (b), we found that the interaction leads to the formation of a localized empty level below the polymer LUMO level. The localized intragap level is calculated to be 0.5 eV below the LUMO level for (NDI2OD-T2)$_1$ and 0.34 eV below the LUMO level for (NDI2OD-T2)$_5$ (Figure 6a).

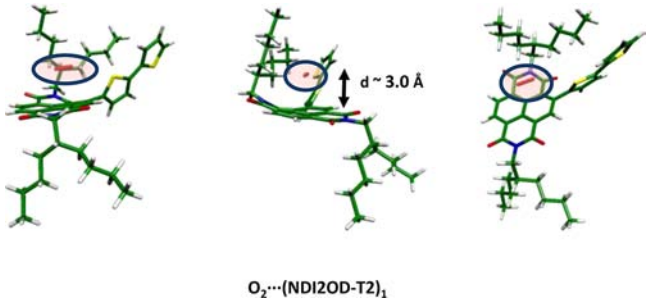

Figure 5. DFT (M06-2X-6-311G**) optimized O_2···(NDI2OD-T2)$_1$ complex structure shown from different perspectives. The optimized intermolecular equilibrium distance between O_2 and NDI core is shown, and the interacting oxygen molecule is highlighted with a circle.

The fundamental charge transport levels for studying the charge transport processes in organic materials are the HOMO and LUMO levels, their energy, symmetry (shape), and couplings in molecular aggregates or crystals.[43−45] In this case, we limit our analysis on the energy and shape of the molecular orbitals involved in the interaction with molecular oxygen. In Figure 6b, we report the frontier molecular orbitals for (NDI2OD-T2)$_5$ before (isolated) and after (molecular complex) the O_2 interaction. In the isolated, pristine molecule, the HOMO wave function is localized mainly on the bithiophene group involving mainly two/three repeat units, while LUMO is localized on the NDI2OD core (spreading over two/three repeat units). Once O_2 interacts with the polymer, an intragap level, with energy lower (∼0.34 eV) than the polymer-LUMO, is created.[46] This intragap orbital is mainly localized on the O_2 molecule with a small electronic coupling with the interacting NDI unit. While the HOMO orbital is slightly affected by the interaction with the molecular oxygen (same shape, delocalization, and small energy shift 0.22 eV), the LUMO is much affected, thus changing its shape (coupling with the antibonding orbital of O_2) and energy (0.24 eV, see Figure 6b).

The intragap level induced by the stabilized interaction between polymer and oxygen has all of the characteristics of the trapping site described in the Experimental Section: The energy of the intragap level is lower than that of the electron transport polymer level (LUMO), and the non-negligible electronic coupling with the NDI π-electrons will increase the trapping rate on the oxygen molecule. Furthermore, the O_2−polymer interaction induces an energy reorganization of the frontier molecular orbitals (slight changes in the HOMO and LUMO energy), thus resulting in shifts as those observed by the CAS spectra.[30] The calculated electronic transitions from the ground state (S_0) to the low lying singlet (dipole allowed) excited states (S_0→S_1, S_0→S_2), reported in the Supporting Information (Figure S1), are in fact red-shifted and blue-shifted, respectively, matching the results obtained by CAS as reported in Figure 4. The mainly triplet character of the oxygen orbitals involved in the formation of the trap level, together with the small overlap with the polymer HOMO, makes the optical transition between the two states not allowed, as shown by the negligible oscillator strength reported in the Supporting Information (Table S1) calculated for the first excited-state transition. This provides an explanation why the electrons

dx.doi.org/10.1021/ja304198e | J. Am. Chem. Soc. 2012, 134, 14877−14889

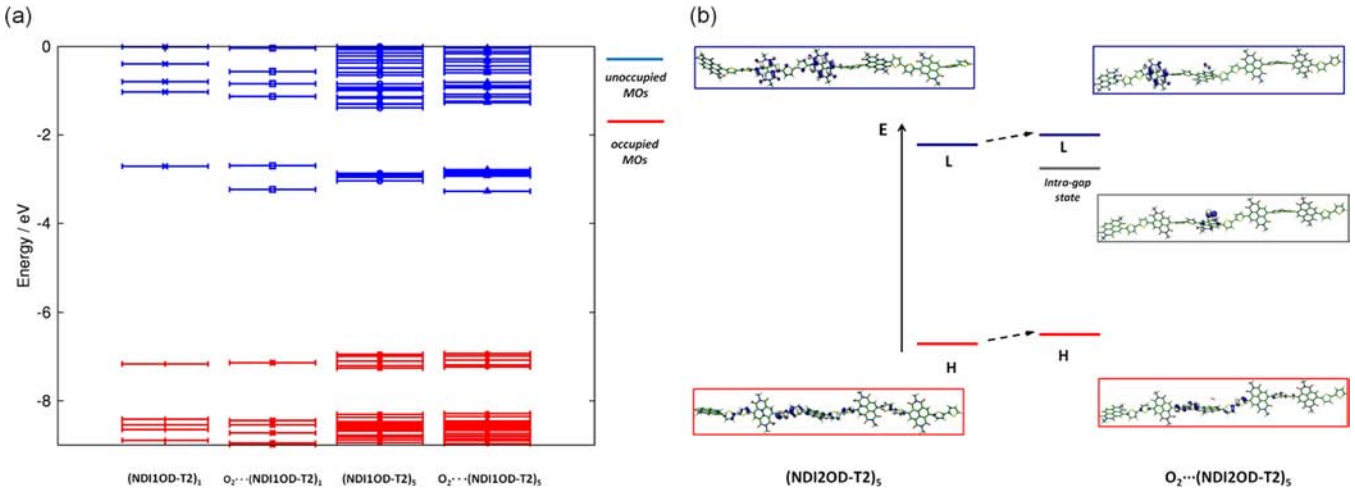

Figure 6. (a) Molecular orbital energy levels as calculated at the M06-2X/6-311G** for the polymer alone and for the polymer···oxygen complex. On the left is shown the calculation for the monomer (e.g., $(NDI2OD\text{-}T2)_1$ and $(NDI2OD\text{-}T2)_1\cdots O_2$) and on the right for the five repeat unit oligomer (e.g., $(NDI2OD\text{-}T2)_5$ and $(NDI2OD\text{-}T2)_5\cdots O_2$). (b) Frontier molecular orbitals (HOMO, LUMO, and intragap orbital) for the five unit oligomer and oxygen complex and a sketch of the energy level reorganization upon oxygen interaction.

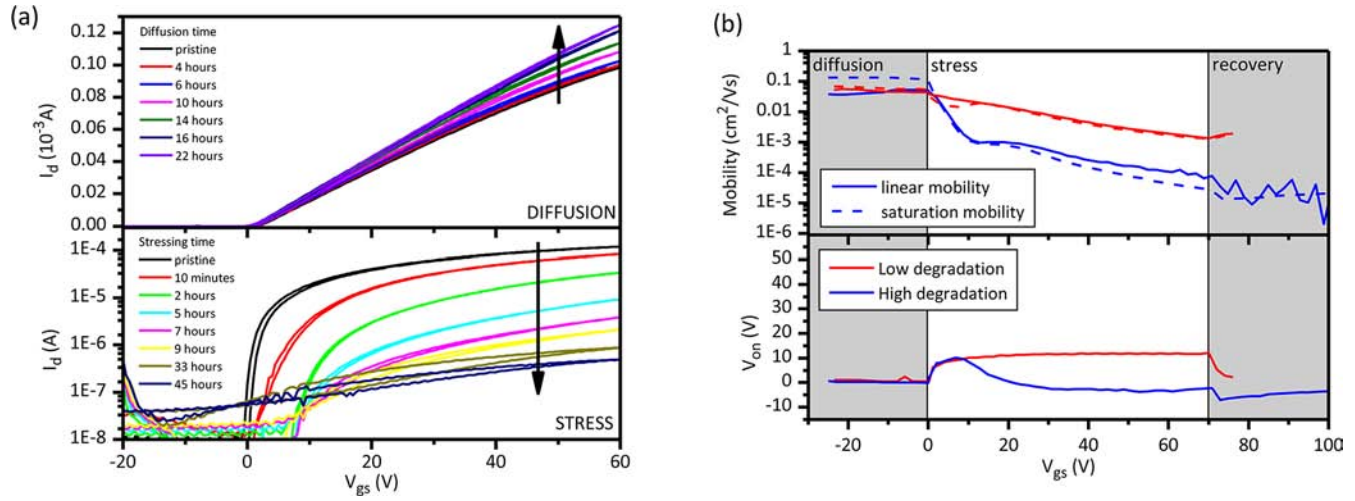

Figure 7. (a) Effect of H_2O diffusion (top graph) and bias stress (bottom graph) on the linear transfer characteristics, shown for the experiment with higher water concentration. (b) Time evolution of mobility (top graph) and onset voltage (bottom graph) for both experiments. The three different phases are outlined at the top of the graph.

trapped on this complex do not exhibit a measurable spectroscopic signature in CAS.

The slight destabilization of the HOMO of the NDI2OD-T2 oligomer will have a beneficial effect on the difficult hole injection, and this might be the reason why with increasing oxygen exposure we observe a hole accumulation signature in the electrical characteristics. For electrons, however, this trap would effectively increase contact resistance due to the increased trapping in the bulk of the polymer, where electron concentration is small, while at least for sufficiently short or low oxygen exposure the electron concentration at the semiconductor–dielectric interface is sufficiently high that a small concentration of traps might not yet reduce materially the saturation mobility extracted at high gate voltages. However, when the density of the oxygen-induced trap site becomes comparable to the charge density in the accumulation layer, the saturation mobility is expected to drop, and hysteresis is expected to increase as observed experimentally. The interaction between molecular oxygen and the neutral polymer can therefore explain the changes observed in the behavior of the device in a dry air atmosphere.

THE ROLE OF WATER

To study the stability of the polymer against water, we performed the same experiment while flushing the cryostat with a mixture of nitrogen gas and water vapor. The mixture was obtained by flowing nitrogen gas through a glass bubbler filled with deionized water. The experiment was repeated twice, with two different devices and with two different concentrations of water (referred to as high and low below) in the gas mixture.

Electrical Characterization. In Figure 7a, the evolution of the linear transfer characteristics for the experiment with higher water concentration is shown. Upon diffusion there is a slight improvement of the linear transfer characteristics, which is not observed in the saturation transfer curves. This effect is not seen in the low water concentration experiment and is probably linked to the different residual oxygen content in this particular sample.

dx.doi.org/10.1021/ja304198e | J. Am. Chem. Soc. 2012, 134, 14877–14889

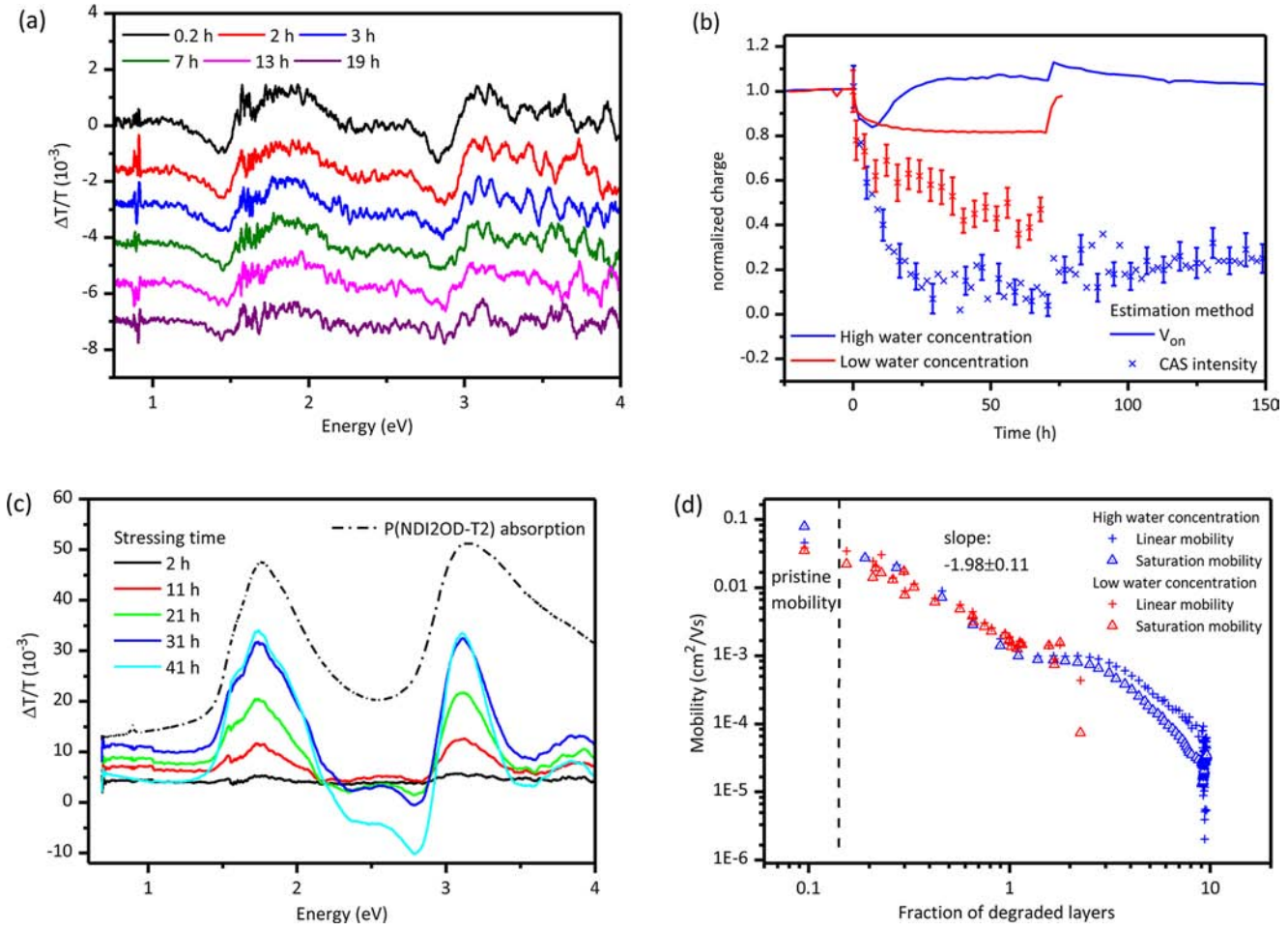

Figure 8. (a) CAS spectra of mobile polarons, obtained at different times during the stress part of the experiment, for the high water concentration experiment. The traces are offset for clarity. (b) Evolution of mobile charge density (line) and charge accumulated on the polymer film (points) during stress and recovery. (c) Trap-sensitive CAS spectra as a function of stressing time in water atmosphere, referenced to the optical spectrum of the device before beginning the stress (t = 0 h). The transmission spectrum of a P(NDI2OD-T2) film (dash−dotted line) is also shown. (d) Correlation between the number of degraded layers and the mobility of the device. Both experiments show the same correlation between the two parameters. The slope of the trace in the first half is reported in the graph. Mobilities reported in the graph are taken at V_{gs} = 55 V.

Upon gate bias application (Figure 7a, bottom graph), the transfer characteristics degrade rapidly. The main effect appears to be a rapid decrease of mobility with only minor onset voltage shift and no increase in hysteresis. In the later stages of device degradation, we observe an increase in the off current as well. The evolution of the transport parameters for both the high water concentration and the low water concentration is plotted in Figure 7b. The graph clearly shows how device degradation is triggered by charge accumulation, because during diffusion in both experiments the device performance was stable, apart from the slight linear mobility increase already explained.

Upon exposure to water, the mobility drops with a similar rate for both linear and saturation regimes, and the rate of degradation is higher for the high water concentration than for the low water concentration. In contrast, the onset voltage increases only little and stabilizes at around +10 V. The subsequent apparent negative shift observed in the high water concentration is caused by an increase in off current, which complicates the extraction of V_{on} from the transfer curve. While the onset voltage seems to recover upon bias removal, there is no recovery of the mobility or the increased off-current in the high water concentration experiment.

The increase of the onset voltage, as we already demonstrated in the case of ambient atmosphere stress, is due to irreversible trapping of some electrons by an electrochemical process. In this case, the trapping is limited to roughly 20% of the accumulated charge, and recovers upon bias removal; that is, the onset voltage returns back to the pristine value.

As pointed out in the Introduction, the P(NDI2OD-T2) polymer should be stable in a H_2O/N_2 environment, when considering the standard half-cell potentials. Yet for the reaction of the radical anion with water reported in Table 1, the redox potential also has a characteristic pH dependence, which is described by the Nernst equation:

$$E = E_0 + 0.0295 \cdot \log \frac{[H_2O]^2[pol^-]^2}{[H_2][pol]^2[OH^-]^2} \quad (3)$$

E_0 = −0.39 V is the standard redox potential calculated from the values reported in Table 1. Although it is difficult to quantify the concentrations of the different species in the accumulation layer of the transistor, it is still easy to see that the full cell potential can become positive for a sufficiently high concentration of H_2O and pol^-. The reaction will then proceed

dx.doi.org/10.1021/ja304198e | J. Am. Chem. Soc. 2012, 134, 14877−14889

until $[OH^-]$ will become high enough to bring the cell potential to 0. This might explain the limited onset voltage shift and the reversibility of the reaction.

Optical Characterization. To characterize the main degradation mechanism in the presence of water that leads to the rapid decrease in mobility, we have again used CAS. The mobile CAS measurements (Figure 8a) performed during the experiment show a decrease of the amount of charge accumulated on the polymer film upon stressing of the device. As happens with the mobility drop, the decrease does not recover during the recovery part of the experiment. In Figure 8b, we compared the amount of mobile charge with the amount of charge accumulated on the polymer film, following the same method employed for the analysis of the dry air measurements. The mismatch between the electrical and the optical estimate is an indication that while the redox reaction can be responsible for part of the charge trapping, they cannot explain entirely the reduction of the charge accumulated on the polymer film. We must conclude that a significant fraction of the charge accumulated in the device upon gate bias application is not located on polymer chains and is not optically active.

To understand the origin of this difference, we acquired CAS spectra in the trap sensitive mode (Figure 8c), using the optical scan obtained before starting the stress (t = 0 h) as a reference. In these spectra, there are three very clear spectral features, two bleaching peaks at 1.7 and 3.1 eV and a new induced absorption band between 2.2 and 2.9 eV (Figure 8c). These spectral features are very intense ($\Delta T/T > 0.03$), while the features due to mobile polarons in the mobile CAS spectra in Figure 8a were far less pronounced ($\Delta T/T < 0.002$). The two bleaching peaks correspond to the neutral absorption peaks of P(NDI2OD-T2), clearly indicating a significant reduction of polymer units that maintain their pristine absorption spectrum. This bleaching is direct evidence for a significant chemical degradation of the polymer induced by the simultaneous presence of water and bias application.

The much higher intensity of the bleaching as compared to what is observed from the "mobile" CAS in Figure 8a indicates that more than one degraded site is formed per accumulated electron. Therefore, the degradation reaction, although involving the negatively charged polymer and water, does not permanently trap the electron. The electron is recycled and induces additional degradation reactions of the polymer with water on other polymer chain segments.

To obtain a quantitative estimate of this degradation, we estimated the absorption cross-section of P(NDI2OD-T2) for photon energies of 1.74 eV from the transmission spectrum (Supporting Information, Figure S3) of a 40 ± 5 nm thick film on spectrosil, using

$$T = e^{-tk},\ k = \sigma n \tag{4}$$

where t is the thickness of the optically active layer, k (the extinction coefficient) is the product of the cross-section, σ, and the density of monomer units of the polymer in the film, is n. Because no detailed unit cell parameters are available, we used an estimate of the unit cell volume $V_{unit} = 1.4 \times 10^{-21}$ cm^3 from the literature.[47] We then used the calculated cross-section, $\sigma = (1.8 \pm 0.4) \times 10^{-16}$ cm^2 to determine the optical thickness of bleached polymer. From the Beer–Lambert law, we derived the following formula:

$$\frac{\Delta T}{T} = e^{\sigma \Delta n t} - 1 \tag{5}$$

where $\Delta T/T$ is evaluated at the peak value of 1.74 eV, and Δn is the density of degraded polymer sites. By assuming that all degradation occurs near the interface, where the electron concentration is highest, we can express the change in transmission in terms of the fraction of degraded polymer monolayers at the interface. This assumption is reasonable because degradation is triggered by charge accumulation and hence is taking place only in the channel area of the device. We assume further a face-on configuration, and consider the π-stacking distance of 3.9 Å as the thickness of a monolayer. This is only a crude approximation because the polymer layer is not fully crystalline.[48]

We plotted the mobility of the two devices against the density of degraded sites in Figure 8d. This result shows a clear correlation between the chemical degradation of the polymer and the decrease in mobility. We observe a plateau in mobility degradation when a full monolayer has been degraded. The origin of this is not clear, but we note how transport after this step can be considered as taking place mostly through degraded polymer sites. This is also confirmed from the mobile CAS spectra, which at this point show almost no mobile polaron signature on the pristine polymer chains anymore.

The relationship between the drop in mobility and the thickness t of the degraded layer, in the first part of the plot, follows approximately an inverse square law:

$$\mu \propto \frac{\mu_0}{t^2} \tag{6}$$

In the standard mobility edge model, effective mobility is inversely dependent on the density of trap states.[49] This is because, although the mobility in the conduction band for transport between trapping event is assumed to be not affected by traps, the total time spent in traps is proportional to the trap site density. Our measurement suggests that for such high densities of trap states, also the mobility for transport between trapping events is affected, possibly because the significant number of chemically degraded sites reduces the number of hopping sites available for transport.

To understand the chemical nature of the degraded species, we performed Raman spectroscopy measurements on the degraded devices (Figure 9). Because the degradation is triggered by charge accumulation, it is possible to obtain the Raman spectrum of the pristine film on the same substrate as the degraded device by acquiring it off the active area, that is, outside the gate electrode area (this spectrum has also been checked against a pristine device and found to be comparable, which provides additional evidence of degradation being triggered by charge accumulation). The Raman spectrum of a device degraded by simultaneous water exposure and bias stress was obtained by shining the laser through the semitransparent gate electrode. We observe a generally similar Raman spectrum to that obtained off the active area; however, we detected a subtle difference in the relative intensities of the three peaks in the 1400–1500 cm^{-1} spectral range. In the degraded sample (top blue trace), the middle peak (at 1436 cm^{-1}) has a higher intensity relative to the adjacent lower and higher frequency peaks than in the spectrum from the pristine material (top red trace).

In these experiments, it was not possible to compare the absolute intensities because the laser is attenuated by the gate electrode (hence the increased noise in the degraded sample trace). To address this problem, we stripped off the PMMA

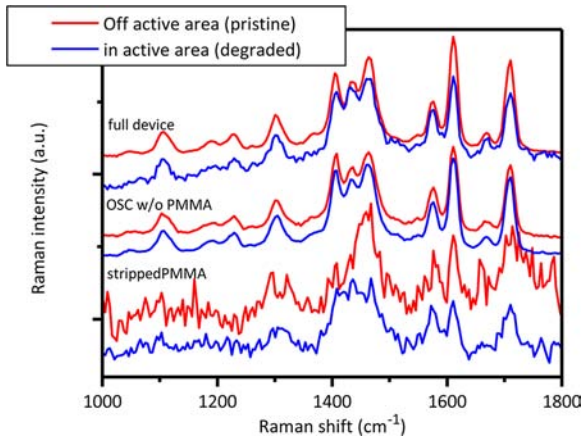

Figure 9. Raman spectra of the high water content sample after the bias stress experiment. The top two traces (full device) refer to Raman spectra collected from the device through the gate and dielectric layer (in active area) and outside the gate area through the dielectric layer (off active area). The two middle traces (OSC w/o PMMA) refer to the spectra obtained from the organic semiconductor (OSC) film after removing the gate and dielectric layers with adhesive tape. The bottom two traces (stripped PMMA) were collected from the exposed dielectric surface.

gate dielectric using adhesive tape and investigated the surface of the P(NDI2OD-T2) film in the active area directly.

The spectra taken from outside and inside the active area in this case have very similar intensities, but the shapes of the spectra are now identical (middle traces). We then measured the Raman spectrum of the exposed surface of the stripped PMMA layer to check whether some P(NDI2OD-T2), responsible for the change in Raman intensities, might have remained stuck to the surface of PMMA during the removal process. Indeed, the two corresponding spectra (bottom) both show the presence of the polymer on the PMMA, although the intensity is reduced by the lack of a reflecting layer that helps light collection (all other spectra were acquired from positions over the source-drain contacts) and the much smaller quantity of material remaining on the exposed PMMA. The spectra taken on the adhesive tape/PMMA structure showed a much higher background scattering than did the other spectra. We removed the background using an 8-points user defined spline curve (defined on areas where no peaks where present), and normalized the intensity to compare the spectra with the ones collected from the pristine device. Although the signal-to-noise level of the polymer spectra taken from the stripped PMMA prevents any quantitative analysis, it is possible to notice how the shape of the spectrum in the 1400−1500 cm^{-1} range is different inside and outside the active area, and that the spectrum from the active area is similar to that seen by taking spectra through the gate electrode (top blue trace).

These Raman data provide evidence that there is indeed an interfacial layer of P(NDI2OD-T2) that is chemically degraded by the application of a bias stress while exposed to moisture. In the experiment on the polymer film, after stripping off the PMMA, we have most likely removed most of the degraded interface layer with the PMMA, and this is why no difference is detected. The Raman spectra measured on the interfacial layer of P(NDI2OD-T2) that is stripped off with the PMMA show a clear spectral difference, providing evidence for the bias stress-induced degradation of the polymer. Unfortunately, the low signal-to-noise ratio of the measurements on the stripped PMMA films prevents us from interpreting more quantitatively the subtle differences observed on the full device.

From the literature, it is possible to associate the three peaks in the Raman spectra under investigation with the naphthalene diimide group of the polymer.[50−52] The fact that the LUMO level is mainly localized on the NDI unit and that the degradation reaction is taking place between the charged polymer unit and water molecules, together with the changes in the relative intensity of the Raman peaks, strongly indicates that it is on this unit that the degradation reaction takes place and where the backbone conjugation is disrupted.

■ CONCLUSIONS

We studied the stability of P(NDI2OD-T2) under different conditions, by combining electrical characterization of the device behavior with simultaneous, spectroscopic characterization by CAS. The findings have been confirmed using quantum chemical calculations and Raman spectroscopy. We studied separately electron trapping and device degradation due to chemical interactions of the polymer with O_2 and H_2O, respectively. Oxygen exposure has been found responsible for a mobility decrease in air caused by the formation of a localized electronic level below the LUMO of the polymer, which acts as a shallow trap for electrons. This particular interaction involves the neutral polymer and is due to a stabilizing interaction between oxygen and the polymer. From quantum chemical calculations, we conclude that the fused benzene ring structure of the naphthalene diimide unit is responsible for the stabilizing interaction with the electronic density of the oxygen molecule. In the presence of water only, we observed two competing degradation mechanisms: an electron transfer process, which due to the low LUMO energy of the semiconducting polymer has only a limited effect and is reversible, and an irreversible chemical degradation of the polymer film, again involving the naphthalene diimide unit of the polymer. It is interesting to note that this water-induced degradation reaction has not previously been observed in air. We presume that this is because in the presence of both oxygen and water, the electrochemical oxidation of the polymer anion is so rapid that the water-induced chemical degradation of the polymer is effectively suppressed. This might suggest as well that in ambient atmosphere, the formation of the shallow oxygen-induced trapping level might be the initial step for the electron transfer process leading to the deep trapping of the electron on the hydroxyl ion.

The degradation pathways observed here are caused by the structure of the electronic orbitals of naphthalene diimide and molecular oxygen (in its triplet state) and water, respectively, and not by the particular energy of the LUMO level[22] or the particular choice of comonomers. It appears likely that the insight gained in the present work is more generally relevant to other rylene diimide-based polymers and molecules. We note that many other polymer or small molecule systems based on naphthalene diimide[5,20] and perylene diimide[22,53,54] have been reported to exhibit similar mobility degradation upon oxygen exposure. It is also possible that the specific mechanisms for electron trapping observed here are relevant to a wider range of conjugated organic materials, including those comprising acene or fused ring imide functional groups, such as diketopyrrolopyrroles (DPPs).[55,56] We note, for example, that a similar interaction with oxygen has recently been studied theoretically in the case of picene.[30] Corresponding CAS investigations are underway.

While our results show that a lower LUMO level is indeed desirable for the electrochemical stability of the polymer semiconductor, they also point out that the stability of these materials cannot be reduced simply to a problem of electron energy on the polymer chain, and that the local structure of the polymer has an important role in determining whether a reaction will be allowed or forbidden. In any material, a careful study of all of the stages of the electron transfer process and of the complex interaction between the polymer and the different molecular species in the atmosphere will be needed to achieve the goal of stable ambient air operation. Besides lowering the LUMO level of the semiconducting molecule and preventing the diffusion of contaminants in the thin film, our study shows how a careful characterization of the different degradation mechanisms can help in understanding which chemical units are responsible for air instability and which are stable. This provides important insight for the design of air-stable electron transporting materials. In this respect, our newly developed technique, CAS, has shown its potential in identifying the origin of the degradation observed in the electrical behavior and has proven to be an extremely useful technique in understanding trapping and atmosphere/bias stress-induced degradation of electron transport in polymer semiconductors.

■ ASSOCIATED CONTENT

Supporting Information

P(NDI2OD-T2) excited-state calculation, including Table S1 listing oscillator strengths and Figures S1 and S2 showing calculated TDDFT excited-state transitions for the polymer alone and for the polymer+O_2 complex; Figure S3, the absorption spectrum of P(NDI2OD-T2) film; and Cartesian coordinates of the optimized P(NDI2OD-T2)$_n$ (both n = 1 and n = 5 oligomers). This material is available free of charge via the Internet at http://pubs.acs.org.

■ AUTHOR INFORMATION

Corresponding Author

hs220@cam.ac.uk

Notes

The authors declare no competing financial interest.

■ ACKNOWLEDGMENTS

We gratefully acknowledge funding from the Engineering and Physical Sciences Research Council (EPSRC), the Cambridge Integrated Knowledge Center (CIKC), and the Hitachi Cambridge Laboratory. We would like to thank Mr. Roger Beadle for his help in building the experimental setup used for the optical absorption and electrical measurement presented in this work.

■ REFERENCES

(1) Paloheimo, J.; Isotalo, H.; Kastner, J.; Kuzmany, H. *Synth. Met.* **1993**, *55*, 3185−3190.
(2) Haddon, R. C.; Perel, A. S.; Morris, R. C.; Palstra, T. T. M.; Hebard, A. F.; Fleming, R. M. *Appl. Phys. Lett.* **1995**, *67*, 121−123.
(3) Facchetti, A.; Deng, Y.; Wang, A.; Koide, Y.; Sirringhaus, H.; Marks, T. J.; Friend, R. H. *Angew. Chem., Int. Ed.* **2000**, *112*, 4721−4725.
(4) Bao, Z. A.; Lovinger, A. J.; Brown, J. *J. Am. Chem. Soc.* **1998**, *120*, 207−208.
(5) Katz, H. E.; Lovinger, A.; Johnson, J.; Kloc, C.; Siegrist, T.; Li, W.; Lin, Y.; Dodabalapur, A. *Nature* **2000**, *404*, 478−81.
(6) Jones, B. A.; Ahrens, M. J.; Yoon, M.-H.; Facchetti, A.; Marks, T. J.; Wasielewski, M. R. *Angew. Chem., Int. Ed.* **2004**, *116*, 6523−6526.
(7) Wang, Z.; Kim, C.; Facchetti, A.; Marks, T. J. *J. Am. Chem. Soc.* **2007**, *129*, 13362−13363.
(8) Jones, B. A.; Facchetti, A.; Marks, T. J.; Wasielewski, M. R. *Chem. Mater.* **2007**, *19*, 2703−2705.
(9) Sirringhaus, H. *Adv. Mater.* **2009**, *21*, 3859−3873.
(10) de Leeuw, D. M.; Simenon, M. M. J.; Brown, A. R.; Einerhand, R. E. F. *Synth. Met.* **1997**, *87*, 53−59.
(11) Arkhipov, V. I.; Heremans, P.; Emelianova, E. V.; Adriaenssens, G. J.; Bässler, H. *Appl. Phys. Lett.* **2003**, *82*, 3245−3247.
(12) Trasatti, S. *Pure Appl. Chem.* **1986**, *58*, 955−966.
(13) Parker, V. D. *J. Am. Chem. Soc.* **1976**, *98*, 98−103.
(14) Anthopoulos, T. D.; Anyfantis, G. C.; Papavassiliou, G. C.; de Leeuw, D. M. *Appl. Phys. Lett.* **2007**, *90*, 122105.
(15) Facchetti, A.; Yoon, M. H.; DiBenedetto, S. A.; Marks, T. J. *J. Am. Chem. Soc.* **2005**, *127*, 1348−1349.
(16) Malenfant, P. R. L.; Dimitrakopoulos, C. D.; Gelorme, J. D.; Kosbar, L. L.; Graham, T. O.; Curioni, A.; Andreoni, W. *Appl. Phys. Lett.* **2002**, *80*, 2517.
(17) Anthony, J. E.; Facchetti, A.; Heeney, M.; Marder, S. R.; Zhan, X. *Adv. Mater.* **2010**, *22*, 3876−92.
(18) Usta, H.; Risko, C.; Wang, Z.; Huang, H.; Deliomeroglu, M. K.; Zhukhovitskiy, A.; Facchetti, A.; Marks, T. J. *J. Am. Chem. Soc.* **2009**, *131*, 5586−608.
(19) Jones, B. A.; Facchetti, A.; Wasielewski, M. R.; Marks, T. J. *J. Am. Chem. Soc.* **2007**, *129*, 15259−15278.
(20) Jung, B. J.; Lee, K.; Sun, J.; Andreou, A. G.; Katz, H. E. *Adv. Funct. Mater.* **2010**, *20*, 2930−2944.
(21) Guo, X.; Ortiz, R. P.; Zheng, Y.; Hu, Y.; Noh, Y.-Y.; Baeg, K.-J.; Facchetti, A.; Marks, T. J. *J. Am. Chem. Soc.* **2011**, *133*, 1405−1418.
(22) Weitz, R. T.; Amsharov, K.; Zschieschang, U.; Villas, E. B.; Goswami, D. K.; Burghard, M.; Dosch, H.; Jansen, M.; Kern, K.; Klauk, H. *J. Am. Chem. Soc.* **2008**, *130*, 4637−4645.
(23) Mathijssen, S. G. J.; Cölle, M.; Gomes, H.; Smits, E. C. P.; de Boer, B.; McCulloch, I.; Bobbert, P. A.; de Leeuw, D. M. *Adv. Mater.* **2007**, *19*, 2785−2789.
(24) Di Pietro, R.; Sirringhaus, H. *Adv. Mater.* **2012**, *24*, 3367−3372.
(25) Chen, Z. H.; Zheng, Y.; Yan, H.; Facchetti, A. *J. Am. Chem. Soc.* **2009**, *131*, 8−9.
(26) Yan, H.; Chen, Z.; Zheng, Y.; Newman, C.; Quinn, J. R.; Dötz, F.; Kastler, M.; Facchetti, A. *Nature* **2009**, *457*, 679−86.
(27) Zhao, Y.; Truhlar, D. G. *Theor. Chem. Acc.* **2007**, *120*, 215−241.
(28) Boys, S. F.; Bernardi, F. *Mol. Phys.* **1970**, *19*, 553−566.
(29) Fazzi, D.; Caironi, M.; Castiglioni, C. *J. Am. Chem. Soc.* **2011**, *133*, 19056−19059.
(30) Caironi, M.; Bird, M.; Fazzi, D.; Chen, Z.; Di Pietro, R.; Newman, C.; Facchetti, A.; Sirringhaus, H. *Adv. Funct. Mater.* **2011**, *21*, 3371−3381.
(31) Wang, Y.; Di Motta, S.; Negri, F.; Friedlein, R. *J. Am. Chem. Soc.* **2011**, *133*, 10054−10057.
(32) Frisch, M. J.; et al. *Gaussian 09*, revision A.1; Gaussian, Inc.: Pittsburgh, PA, 2009.
(33) Vissenberg, M. C. J. M.; Matters, M. *Phys. Rev. B* **1998**, *57*, 12964−12967.
(34) Chesterfield, R. J.; Mckeen, J. C.; Newman, C. R.; Ewbank, P. C.; da Silva Filho, D. A.; Brédas, J.-L.; Miller, L. L.; Mann, K. R.; Frisbie, C. D. *J. Phys. Chem. B* **2004**, *108*, 19281−19292.
(35) Hoppe, A.; Balster, T.; Muck, T.; Wagner, V. *Phys. Status Solidi A* **2008**, *205*, 612−625.
(36) Pesavento, P. V.; Puntambekar, K. P.; Frisbie, C. D.; McKeen, J. C.; Ruden, P. P. *J. Appl. Phys.* **2006**, *99*, 094504.
(37) Minari, T.; Nemoto, T.; Isoda, S. *J. Appl. Phys.* **2004**, *96*, 769.
(38) Ucurum, C.; Goebel, H.; Yildirim, F. a.; Bauhofer, W.; Krautschneider, W. *J. Appl. Phys.* **2008**, *104*, 084501.
(39) Petit, C.; Zander, D.; Lmimouni, K.; Ternisien, M.; Tondelier, D.; Lenfant, S.; Vuillaume, D. *Org. Electron.* **2008**, *9*, 979−984.
(40) Stallinga, P.; Gomes, H. L.; Biscarini, F.; Murgia, M.; de Leeuw, D. M. *J. Appl. Phys.* **2004**, *96*, 5277.

(41) Ferretti, A. *Coord. Chem. Rev.* **2003**, *238*−*239*, 127−141.
(42) Bublitz, G. U.; Boxer, S. G. *Annu. Rev. Phys. Chem.* **1997**, *48*, 213−242.
(43) McMahon, D. P.; Troisi, A. *ChemPhysChem* **2010**, *11*, 2067−74.
(44) Troisi, A. *Chem. Soc. Rev.* **2011**, *40*, 2347−58.
(45) Fazzi, D.; Castiglioni, C.; Negri, F. *Phys. Chem. Chem. Phys.* **2010**, *12*, 1600−1609.
(46) McMahon, D. P.; Troisi, A. *Phys. Chem. Chem. Phys.* **2011**, *13*, 10241−8.
(47) Rivnay, J.; Toney, M. F.; Zheng, Y.; Kauvar, I. V.; Chen, Z.; Wagner, V.; Facchetti, A.; Salleo, A. *Adv. Mater.* **2010**, *22*, 4359−4363.
(48) Rivnay, J.; Noriega, R.; Kline, R.; Salleo, A.; Toney, M. *Phys. Rev. B* **2011**, *84*, 045203.
(49) Street, R. A. *Hydrogenated Amorphous Silicon*; Cambridge University Press: UK, 2005.
(50) Stenman, F. *J. Chem. Phys.* **1971**, *54*, 4217.
(51) Aroca, R. F.; Alvarez-Puebla, R. A.; Pieczonka, N.; Sanchez-Cortez, S.; Garcia-Ramos, J. V. *Adv. Colloid Interface Sci.* **2005**, *116*, 45−61.
(52) Schuettfort, T.; Huettner, S.; Lilliu, S.; Macdonald, J. E.; Thomsen, L.; McNeill, C. R. *Macromolecules* **2011**, *44*, 1530.
(53) Wen, Y.; Liu, Y.; Di, C.; Wang, Y.; Sun, X.; Guo, Y.; Zheng, J.; Wu, W.; Ye, S.; Yu, G. *Adv. Mater.* **2009**, *21*, 1631−1635.
(54) Weitz, R. T.; Amsharov, K.; Zschieschang, U.; Burghard, M.; Jansen, M.; Kelsch, M.; Rhamati, B.; van Aken, P. A.; Kern, K.; Klauk, H. *Chem. Mater.* **2009**, *21*, 4949−4954.
(55) Briseno, A. L.; Kim, F. S.; Babel, A.; Xia, Y.; Jenekhe, S. A. *J. Mater. Chem.* **2011**, *21*, 16461.
(56) Li, Y.; Sonar, P.; Singh, S. P.; Zeng, W.; Soh, M. S. *J. Mater. Chem.* **2011**, 10829.